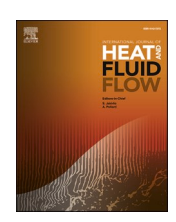
ELSEVIER

Contents lists available at ScienceDirect

International Journal of Heat and Fluid Flow

journal homepage: www.elsevier.com/locate/ijhff





A novel inventory decoupling control strategy for sCO₂ cycle based on the net power superposition principle

Cheng Chang a, Enhui Sun a, o, Jinliang Xu a, Xiaoming Zhang a, Huan Ye b, Qichen Qian a

- a Key Laboratory of Power Station Energy Transfer Conversion and System. North China Electric Power University, Ministry of Education, Beijing 102206, China
- b State Key Laboratory of Low-carbon Thermal Power Generation Technology and Equipments, Harbin Boiler Company Limited, Harbin 150046, China

ARTICLE INFO

Keywords:
Supercritical carbon dioxide cycle
Part-load performance
Recompression cycle
Control strategy
Thermal efficiency

ABSTRACT

The supercritical carbon dioxide (sCO₂) Brayton cycle has garnered considerable attention due to its exceptional efficiency and compact design. However, owing to grid load requirements, the sCO2 cycle often operates at partload, necessitating an investigation into its performance under such conditions. This paper employs the net power superposition principle and mathematical derivations based on the recompression cycle to address this need. Introducing a novel strategy, termed the inventory decoupling control strategy, enhances cycle thermal efficiency at part-load. By splitting the recompression cycle into two simple Brayton cycles and implementing independent inventory control strategies during load adjustment, thermal efficiency at part-load is significantly improved. A 20 MW sCO₂ cycle model incorporating this innovative part-load control strategy was developed for this study. Calculations demonstrate that the inventory decoupling control strategy offers notable efficiency advantages, with a thermal efficiency difference of up to 1.21 % at 30 % load. The primary rationale behind this novel control strategy is to redistribute the regenerative process, thereby enhancing net power superposition and reducing heat dissipation from the cooler during part-load operation. Additionally, the novel control strategy results in less variation in compressor efficiency, leading to higher overall compressor efficiency and enhanced safety. This approach further extends the applicability of the net power superposition principle and explores the potential of inventory control strategies, offering a new perspective for investigating control strategies of sCO2 cycles under part-load conditions.

1. Introduction

Supercritical carbon dioxide (sCO₂) is characterized by its safety, environmental friendliness, and natural availability, and has been successfully applied in various industrial and chemical processes (Ehsan et al., 2018). The supercritical carbon dioxide (sCO₂) Brayton cycle is considered a promising next-generation power cycle due to its high thermal efficiency and compact system layout. (Ehsan et al., 2023; Açıkkalp, 2017; Mecheri and Le Moullec, 2016). Its versatility positions it for application across diverse heat source fields, including nuclear energy (Zhang et al., 2021), solar energy (Linares et al., 2020), gas turbine waste heat (Dal Cin et al., 2023), and fuel cell waste heat (Ryu et al., 2020). However, the sCO₂ cycle often faces off-design operational challenges due to fluctuations in external factors and grid load demands, emphasizing the importance of studying part-load performance characteristics.

Currently, there is limited research on the off-design operating

conditions of the sCO₂ cycle, with most studies focusing on the impact of external environmental factors, internal operating parameters and structure, and control strategies. Concerning the influence of the external environment, Ehsan et al., (Ehsan et al., 2020; Monjurul Ehsan et al., 2020) conducted design analyses of the cooling systems for both recompression and partial cooling sCO2 cycles. Their results indicated that the recompression cycle exhibits higher thermal efficiency under varying sCO2 inlet temperatures to the cooling tower and fluctuating ambient temperatures. They concluded that, for the future commercialization of dry-cooled sCO₂ power plants, the recompression cycle is preferable due to its superior performance and lower costs associated with cooling tower design and solar field infrastructure. Furthermore, Ehsan et al. (Ehsan et al., 2018) performed simulation studies on dry natural draft cooling towers under different external environmental conditions. The results demonstrated that the sCO2 inlet temperature and system operating pressure significantly influence cooling system performance, and that cooling capacity substantially decreases during high ambient temperature periods. In addition, Ehsan et al. (Ehsan et al.,

E-mail address: ehsun@ncepu.edu.cn (E. Sun).

 $^{^{\}ast}$ Corresponding author.

Nomenclature Acronym:		15		
		C1	main compressor	
h	specific enthalpy, kJ/kg	C2	recompressor	
P	pressure, MPa	HTR	high temperature recuperator	
q	heat transfer per unit mass flow rate, kJ/kg	HTR(a)	high temperature recuperator in SC1	
$q_{ m m}$	mass flow rate, kg/s	HTR(b)	high temperature recuperator in SC2	
T	temperature, °C	IC	inventory control	
w	work done per unit mass flow rate, kJ/kg	IDC	inventory decoupling control	
x	split ratio of flow rate	LTR	low temperature recuperator	
Δh	enthalpy drop, kJ/kg	LTR(a)	low temperature recuperator in SC1	
ΔP	pressure drop, MPa	LTR(b)	low temperature recuperator in SC2	
0.1		PCHE	print circuit heat exchanger	
Subscript		RC	Recompression cycle	
	state points of cycle	SC	simple Brayton cycle	
C	compressor	sCO_2	supercritical carbon dioxide	
C1	main compressor	T	turbine 1	
C2	recompressor	T1(a)	turbine 1 in SC1	
c	cool	T1(b)	turbine 1 in SC2	
d	design operating conditions	V	valve	
h	hot	0 1	1 1	
od	off-design operating conditions		Greek symbols	
RC	recompression cycle	$\eta_{ m th}$	thermal efficiency	
T	turbine	$\eta_{ m T}$	isentropic efficiency of turbine	
		$\eta_{ m C}$	isentropic efficiencies of compressor	

2019; Monjurul Ehsan et al., 2020) evaluated the performance of dry cooling systems coupled with concentrating solar power (CSP) plants under various seasonal climates. Their findings highlighted that the design parameters of dry cooling systems have a critical impact on both the CSP plant and its off-design performance across different climatic conditions. Incorporating an additional bypass section upstream of the cooling tower was identified as an effective technique to maintain optimal cycle operation. Floyd et al. (Floyd et al., 2013) investigated how system performance is affected by variations in cooler outlet temperature across seasons and proposed adjusting compressor speed to adapt to changes in environmental temperature. Similarly, Duniam et al. (Duniam and Veeraragavan, 2019) arrived at similar conclusions in their research. Correa et al. (Correa et al., 2021) assessed the effects of variations in heat source and environmental temperature on system performance, noting that adjusting the split ratio can significantly mitigate these impacts. It can be observed that current research primarily addresses environmental variations by adjusting different components and cycle parameters. However, a unified theoretical approach has not yet been proposed.

Regarding the influence of internal operating parameters and structure, Gini et al. (Gini et al., 2023) investigated the part-load characteristics of the simple Brayton cycle and concluded that the sCO₂ mass flow rate plays a crucial role in regulating cycle output power, with the two parameters exhibiting an almost linear relationship. Zheng et al. (HaoNan et al., 2024) analyzed the performance degradation mechanism of the system at part-load, revealing that a reduction in load positively affects system performance through the recuperator, while the turbomachinery exerts a detrimental influence. Yang et al. (Yang et al., 2020) conducted a comparative analysis of the part-load performance among the four most typical sCO2 cycle layouts. Their findings indicated that the recompression cycle demonstrates the highest efficiency at part-load, whereas the intercooling cycle does not offer significant efficiency advantages at low loads. Additionally, Ma et al. (Ma et al., 2022) compared the part-load performance of a simple Brayton cycle with that of a recompression cycle, highlighting the latter's broader regulation range and higher efficiency. It can be seen that previous studies have analyzed the effects of various internal parameters on cycle performance and provided corresponding conclusions.

Nevertheless, similar to studies addressing environmental fluctuations, these works lack a generalized theoretical framework to explain the underlying mechanisms behind the observed phenomena.

In terms of control strategies, several researchers (Wang et al., 2022; Li et al., 2020; Ming et al., 2023) have determined that inventory control can lead to higher efficiency and improved safety at part-load. Luu et al. (Luu et al., 2018) observed that while adopting an inventory control strategy during solar net power fluctuations can enhance efficiency, it has limitations and demonstrates significant benefits only during substantial or stable drops in solar power. Singh et al., (Singh et al., 2013) reached a similar conclusion. Moreover, many studies have indicated that inventory control strategies alone may not suffice to meet efficiency and range requirements, prompting researchers to explore the integration of multiple strategies. Heifetz et al. (Heifetz and Vilim, 2015) developed a mixed-mode controller by combining inventory control with turbine bypass control to enhance system efficiency and stability during control strategy transitions. Fan et al. (Fan et al., 2020) proposed a combined sCO2-tCO2 cycle, evaluating various control strategies and ultimately recommending a composite approach integrating inventory control with bypass control to enhance efficiency and regulation range at part-load. Oh et al. (Oh et al., 2017) investigated control strategies for sCO₂ cooled micro modular reactor system, finding that combining core bypass control with inventory control achieves a load range of 0 %-100 % and higher efficiency compared to core bypass control alone. Du et al. (Du et al., 2024) analyzed equipment exergy loss adopting different control strategies, concluding that for optimal balance between safety and efficiency, a strategy combining inventory control and turbine bypass control is advisable. It is evident that most existing studies focus on basic control strategies and evaluate their individual or combined performances. However, research on inventory control remains limited, and the potential of inventory-based strategies has yet to be thoroughly

In summary, current research on the off-design performance of sCO_2 cycles lacks a generalized theoretical framework, limiting the ability to interpret the underlying causes of observed phenomena. Moreover, studies on inventory control under part-load operation are still in an exploratory stage. Although inventory control is widely regarded as a more efficient strategy, most existing research focuses on expanding its

regulation range by combining it with other control methods. There is a lack of investigation into the relationship between the cycle construction process and inventory control, as well as how to further improve efficiency under inventory-based regulation. Therefore, it is essential to identify a common theoretical approach for enhancing efficiency and to further explore the characteristics of inventory control in order to develop more effective part-load strategies. In this work, we integrate the part-load characteristics of the cycle with its construction process. Based on the net power superposition principle, we decouple the cycle and apply independent inventory control strategies to each sub-cycle, ultimately achieving a more efficient part-load control strategy from the perspective of cycle configuration optimization.

This study focuses on a recompression cycle using a generalized heat source. The objective is to explore the potential of inventory control in order to improve the cycle efficiency of sCO₂ systems under part-load conditions. The research methodology combines theoretical derivation with numerical simulations. Specifically, a theoretical method for improving part-load efficiency is first developed, and then validated through simulations. The part-load characteristics of the proposed approach are also analyzed. The structure of the paper is organized as follows: First, through a comprehensive literature review, we identify that current studies on off-design conditions of sCO2 cycles lack a generalized theoretical framework, which limits the depth of explanation for observed phenomena. Additionally, the research on inventory control strategies remains insufficient. In response, we propose a theoretical approach based on the net power superposition principle to improve part-load efficiency, and introduce a novel inventory decoupling control strategy. Finally, simulation results are presented to verify the effectiveness of the proposed method and to further analyze the partload performance of the cycle.

2. Net power superposition principle and inventory decoupling control strategy

In pursuit of a generalized approach to enhancing sCO_2 cycle efficiency, Sun et al. (Sun et al., 2020) and Li et al. (Hangning et al., 2020) introduced the net power superposition principle. By leveraging the first

law of thermodynamics and theoretical derivation, they illustrated how multiple compressions and regeneration can elevate cycle efficiency, thereby catalyzing the development of multi-compression cycles. The net power superposition principle offers a novel perspective for analyzing cycle characteristics and has proven effective in assessing system steady-state conditions. This has prompted exploration of its application in part-load research, leading to the formulation of the inventory decoupling control strategy.

The structure of the recompression cycle is illustrated in Fig. 1(a). Within the RC cycle, the working fluid initially absorbs heat in the heater before entering the turbine for expansion and work generation. Following this, the fluid releases a portion of its heat in the recuperators, subsequently bifurcating into the cooler and the recompressor at the outlet of the LTR low-pressure side, respectively. Upon entry into the cooler, the fluid undergoes cooling before being pressurized in the main compressor, then passing through the LTR to absorb heat and eventually merging with the fluid from the recompressor at the inlet of the HTR high-pressure side. Upon merging, the fluid enters the HTR to absorb additional heat before concluding the thermal cycle by re-entering the heater. Table 1 presents the thermodynamic balance equations for each component within the cycle.

In the RC cycle, the compressor total power consumption $w_{\rm C}$, the turbine work output $w_{\rm T}$, the heat dissipated by cooler $q_{\rm Cooler}$, the heat

 Table 1

 Thermodynamic balance equations for components in the cycle.

Components	Thermodynamic balance equations	
Main compressor	$ \eta_{\text{C1,s}} = \frac{H_{2\text{s}} - H_1}{H_2 - H_1}, W_{\text{C1}} = (1 - x)(H_2 - H_1)q_{\text{m}} $	
recompressor	$ \eta_{\text{C2,s}} = \frac{H_{3\text{s}} - H_8}{H_3 - H_8}, W_{\text{C2}} = x(H_3 - H_8)q_{\text{m}} $	
Turbine	$ \eta_{\text{T1,s}} = \frac{H_5 - H_6}{H_5 - H_6}, W_{\text{T1}} = (H_5 - H_6)q_{\text{m}} $	
Low temperature recuperator	$x = 1 - \frac{H_7 - H_8}{H_3 - H_2}, Q_{LTR} = (H_7 - H_8)q_m$	
High temperature recuperator	$Q_{\rm HTR} = (H_6 - H_7)q_{\rm m}$	
Cooler	$Q_{\text{Cooler}} = (1 - x)(H_8 - H_1)q_{\text{m}}$	
Heater	$Q_{\mathrm{Heater}} = (H_5 - H_4)q_{\mathrm{m}}$	

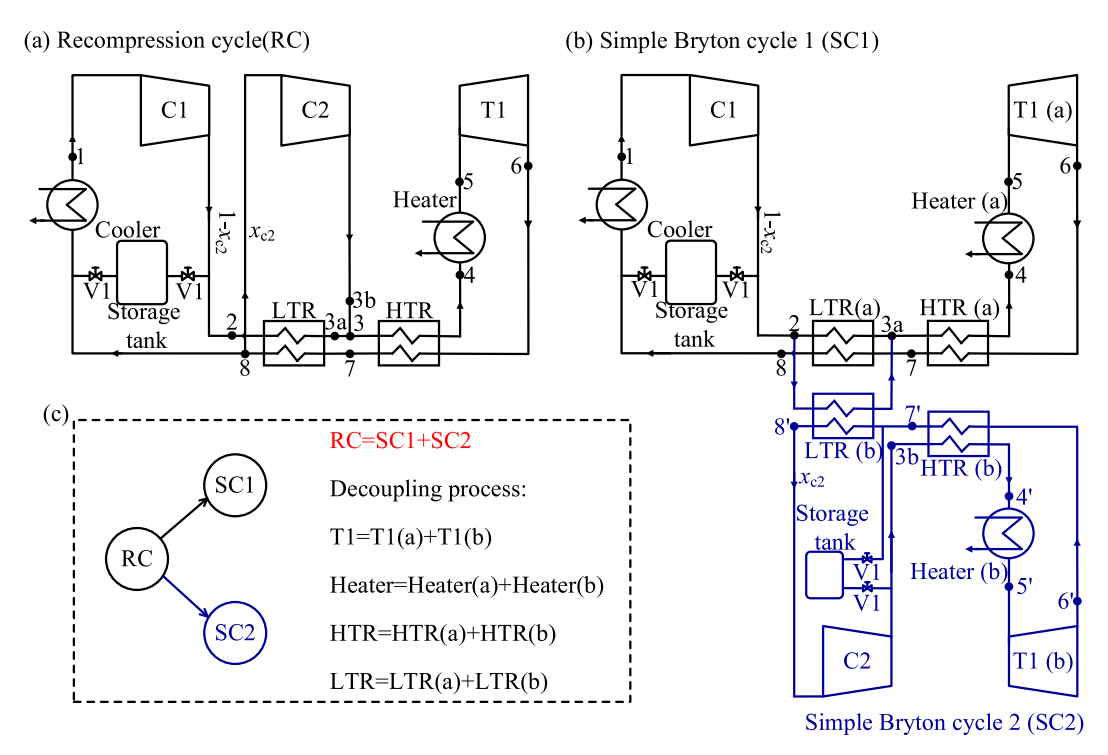


Fig. 1. Schematic diagram of cycles: (a) RC cycle (b) decoupling cycle.

absorption by heater q_{Heater} , and the thermal efficiency $\eta_{\text{th,RC}}$ are:

$$w_{\rm C} = (1 - x_{\rm RC})\Delta h_{\rm C1} + x_{\rm RC}\Delta h_{\rm C2} = (1 - x_{\rm RC})(h_2 - h_1) + x_{\rm RC}(h_{\rm 3b} - h_8)$$
 (1)

$$w_{\mathrm{T}} = \Delta h_{\mathrm{T}} = h_5 - h_6 \tag{2}$$

$$q_{\text{Cooler}} = (1 - x_{\text{RC}})(h_8 - h_1)$$
 (3)

$$q_{\text{Heater}} = \Delta h_{\text{Heater}} = h_5 - h_4 \tag{4}$$

$$\eta_{\text{th,RC}} = \frac{w_{\text{T}} - w_{\text{C}}}{q_{\text{Heater}}} = \frac{\Delta h_{\text{T}} - (1 - x_{\text{RC}})\Delta h_{\text{C1}} - x_{\text{RC}}\Delta h_{\text{C2}}}{\Delta h_{\text{Heater}}}$$
(5)

where $\Delta h_{\rm C1}$ is the main compressor enthalpy change; $\Delta h_{\rm C2}$ is the recompressor enthalpy change; and $\Delta h_{\rm Heater}$ is the heater enthalpy change. According to the first law of thermodynamics, it can be obtained:

$$\Delta h_{\text{Heater}} + (1 - x_{\text{RC}})\Delta h_{\text{C1}} + x_{\text{RC}}\Delta h_{\text{C2}} = (1 - x_{\text{RC}})\Delta h_{\text{Cooler}} + \Delta h_{\text{T}}$$
 (6)

Substitution of Eq. (6) into Eq. (5) gives:

$$\eta_{\rm th,RC} = \frac{w_{\rm T} - w_{\rm C}}{q_{\rm Heater}} = \frac{\Delta h_{\rm T} - (1 - x_{\rm RC}) \Delta h_{\rm C1} - x_{\rm RC} \Delta h_{\rm C2}}{\Delta h_{\rm T} + (1 - x_{\rm RC}) \Delta h_{\rm Cooler} - (1 - x_{\rm RC}) \Delta h_{\rm C1} - x_{\rm RC} \Delta h_{\rm C2}}$$

To simplify the formulation, $\Delta h_{\rm T}$ is divided into two parts:

$$\Delta h_{\rm T} = (1 - x_{\rm RC}) \Delta h_{\rm T} + x_{\rm RC} \Delta h_{\rm T} \tag{8}$$

Substitution of Eq. (8) into Eq. (7) gives:

$$\eta_{\text{th,RC}} = \frac{(1 - x_{\text{RC}})(\Delta h_{\text{T}} - \Delta h_{\text{C1}}) + x_{\text{RC}}(\Delta h_{\text{T}} - \Delta h_{\text{C2}})}{(1 - x_{\text{RC}})(\Delta h_{\text{T}} - \Delta h_{\text{C1}} + \Delta h_{\text{Cooler}}) + x_{\text{RC}}(\Delta h_{\text{T}} - \Delta h_{\text{C2}})}$$
(9)

Eq. (9) is the thermal efficiency of the RC cycle obtained using the splitting method, which can consist of two main parts, the first one is the base cycle term:

$$\frac{(1-x_{\rm RC})(\Delta h_{\rm T}-\Delta h_{\rm C1})}{(1-x_{\rm RC})(\Delta h_{\rm T}-\Delta h_{\rm C1}+\Delta h_{\rm Cooler})} = \frac{(1-x_{\rm RC})(\Delta h_{\rm T}-\Delta h_{\rm C1})}{(1-x_{\rm RC})(\Delta h_{\rm T}-\Delta h_{\rm C1})+(1-x_{\rm RC})\Delta h_{\rm Cooler}}$$
(10)

the second part is the net power superposition term:

$$x_{\rm RC}(\Delta h_{\rm T} - \Delta h_{\rm C2}) \tag{11}$$

According to the net power superposition principle, two key observations can be made:1. If the base cycle term remains constant, a higher value of the net power superposition term (i.e., a larger SC2 net power $x_{\rm RC}(\Delta h_{\rm T} - \Delta h_{\rm c2})$) correlates with higher thermal efficiency. 2. if the net power superposition term is held constant, a larger value of the base cycle term (i.e., a smaller cooler exergy $(1-x_{\rm RC})\Delta h_{\rm Cooler}$) leads to higher thermal efficiency. However, implementing these methods to enhance cycle thermal efficiency is challenging for the recompression cycle. This is because the state parameters at each point of a single cycle deeply affect one another, making it difficult to alter specific parameters without impacting others. The current part-load control strategy is unable to execute the aforementioned approaches.

To address this, we propose decoupling the recompression cycle into two simple Brayton cycles. In this decoupled cycle, SC2 transfers the heat that would have dissipated to the environment to SC1 for regeneration through LTR(b), effectively achieving an equivalent efficiency of 1 for SC2, akin to net power superposition. Fig. 1(b) illustrates the structure of the decoupled cycle, while Fig. 1(c) depicts the construction process. The decoupled cycle operates similarly to the RC cycle, with fluid within SC1 and SC2 completing a thermodynamic cycle through the heater, turbine, recuperator, and cooler. However, in the decoupled cycle, the fluid in SC1 splits at the outlet of the main compressor, with a portion entering LTR(a) to absorb heat and the remainder entering LTR (b) for the same purpose. These two streams converge at the high-pressure inlet of HTR(a), then proceed to HTR(a) and the heater to

absorb heat and complete a thermal cycle. Load regulation of the cycle is achieved through the inventory control strategy (IC), with a $\rm CO_2$ storage tank in each of SC1 and SC2 enabling independent control. This significantly enhances the load control flexibility of the cycle. Consequently, the proposed inventory decoupling control strategy (IDC) allows for the implementation of methods to enhance cycle thermal efficiency without the need for a splitter valve or turbine throttling valve control.

3. System modelling

3.1. Heat exchanger

The heat exchanger utilized in the sCO_2 cycle is a zigzag-type printed circuit plate heat exchanger (PCHE) (Jiang et al., 2018), which is discretized for thermal calculations. Fig. 2 illustrates this discretization, where a single heat exchanger is divided into N subunits. For this study, all 20 subunits of the heat exchanger are selected.

For each subunit interior, it was calculated using the log mean temperature difference (LMTD) method (Jiang et al., 2018), as given in Eq. (12) to Eq. (15).

$$\frac{1}{k} = \frac{1}{h_h} + \frac{\delta}{\lambda} + \frac{A_h}{h_c A_c} \tag{12}$$

$$h_{h/c} = N u_{h/c} \frac{\lambda_{h/c}}{d_{h/c}} \tag{13}$$

$$UA = \frac{Q}{\Delta T_{LMTD}} = \frac{Q}{(\Delta T_{\text{max}} - \Delta T_{\text{min}}) / \ln(\Delta T_{\text{max}} / \Delta T_{\text{min}})}$$
(14)

$$\Delta T_{\text{max}} = \max \left(T_{\text{h,in}} - T_{\text{c,out}}, \ T_{\text{h,out}} - T_{\text{c,in}} \right) \ \Delta T_{\text{min}}$$

$$= \min \left(T_{\text{h,in}} - T_{\text{c,out}}, \ T_{\text{h,out}} - T_{\text{c,in}} \right)$$
(15)

where λ is the heat conductivity of the material; h is the convective heat transfer coefficient in the tube; δ is the equivalent wall thickness; k is the overall heat transfer coefficient of each subunits; A is the heat transfer area; $\lambda_{h/c}$ is the fluid thermal conductivity; Nu is the Nusselt number; and UA is the heat conductance of each subunits.

The pressure drop of each subunits is:

$$\Delta P = \frac{1}{2}\rho G^2 f \frac{L_z}{d} \tag{16}$$

where f is the friction factor; G and ρ denote velocity and density of fluid; d is the hydraulic diameter; and L_z is the channel length of each subunits.

For the CO_2 side and the water side, the correlations between Nu and f are calculated based on the equations provided in references (Jiang et al., 2018) and (Chu et al., 2017), respectively. In this study, the heat exchanger channel corrugation angle is set at 40 degrees, and the construction material chosen is SS316. The sizing follows the guidelines outlined in reference (Pierres et al., 2011), while the initial parameters are as shown in Table 2. During off-design operating conditions, the heat exchanger's structural parameters and inlet parameters are known. The outlet parameters can be obtained through iterative calculations by assuming the pressure drop on both sides and the outlet temperature on the low-pressure side.

In this paper, a generalized heat source is employed for the heater, assuming that it provides ample heat. The pressure drop on the CO₂ side in off-design operating conditions is modeled using the following calculation (Dyreby):

$$\Delta P_{\mathrm{Heater,od}} = \Delta P_{\mathrm{Heater,d}} \left(\frac{q_{\mathrm{m,od}}}{q_{\mathrm{m,d}}}\right)^{7/4}$$
 (17)

where od represents off-design operating conditions; d represents design operating conditions.

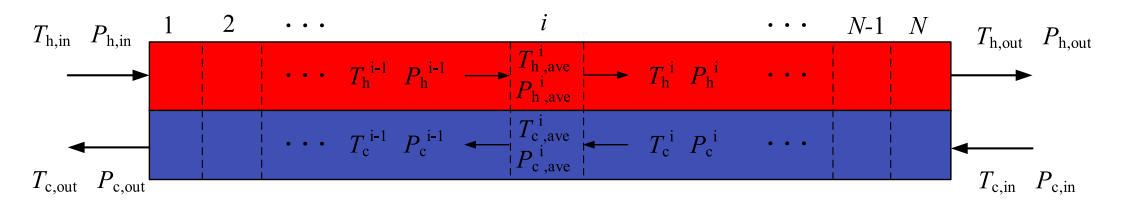


Fig. 2. Schematic of PCHE discrete calculation.

Table 2
PCHE channel parameters.

Parameters	HTR	LTR	Cooler
Channel diameter D _c (mm)	2.00	2.00	2.20
Width between channels t_3 (mm)	0.97	0.80	0.17
Thickness between channels t_2 (mm)	1.02	0.82	0.42
$R_{ m p}$	2	2	1

3.2. Compressor

The compressor model calculation method utilized in this paper is derived from reference (Enhui et al., 2023). This method incorporates enhancements to the loss model, resulting in significantly improved accuracy in predicting compressor performance curves. The modified loss model yields calculation results with smaller errors when compared with experimental data from Sandia Laboratory.

The key formula for the velocity triangle of the inlet is as follows:

$$q_m = \frac{\rho_{0t}(P_{0t}, T_{0t})\pi c_1 D_0^2 (1 - \tau_1)}{4}$$
(18)

$$M_{\text{wsl}} = \frac{\sqrt{c_1^2 + u_{1s}^2}}{c_{\text{sound}}(P_{0t}, T_{0t})}$$
 (19)

$$\tau_1 = 1 - \frac{4Z_1t_1}{\pi(D_{1s} + D_{1h})} \tag{20}$$

where c_1 is the inlet absolute velocity; D_0 , D_s , and D_h denote the equivalent inlet diameter, wheel shroud diameter, and hub diameter; u_{s1} is the tangential velocity at the blade tip; M_{wsl} is the inlet blade tip Mach number; Z_1 is the number of inlet blades; τ_1 is the inlet blockage factor; t_1 is the calculated thickness of the inlet blades; with the subscript 0 denoting the stagnation parameters, and the subscript 1 denoting the inlet of the blades.

The key formula for the velocity triangle of the outlet is as follows:

$$\sigma = 1 - \frac{0.63\pi}{Z_2 \psi} \tag{21}$$

$$\psi = 1 - \phi \cot(\beta_{2A}) - (\pi/Z_2)\sin(\beta_{2A}) \tag{22}$$

$$q_{\rm m} = b_2 \rho_2 c_{\rm 2m} (\pi D_2 - Z_2 t_2) \tag{23}$$

where σ is the slip factor, Z_2 is the number of outlet blades; ψ is the outlet tangential velocity coefficient; D_2 is the outlet impeller diameter; t_2 is the calculated thickness of the outlet blades; with the subscript 2 denoting the outlet of the blades.

In the outlet, inlet, and diffuser calculations incorporating the loss model, compressor performance curves can be obtained. Fig. 3 illustrates the main compressor and recompressor performance curves, where the solid line represents the pressure ratio and the dotted line represents the efficiency.

3.3. Turbine

Due to the relatively high pressure of the CO_2 fluid in the turbine, a multistage axial flow turbine is selected. Off-design calculations of the turbine can be performed using the Stodola elliptic method, which is a model for axial flow turbine off-design operating conditions (Gabbrielli, 2012; Fan and Dai, 2021):

$$\varphi = q_{\rm m,in} \frac{\sqrt{T_{\rm in}}}{P_{\rm in}} \tag{24}$$

$$Y_{\rm d} = \frac{P_{\rm in,d}^2 - P_{\rm out,d}^2}{P_{\rm in,d}^2 \varphi_{\rm d}^2} \tag{25}$$

$$\eta_{\text{T,od}} = \eta_{\text{T,d}} - 2 \cdot \left(\frac{N_{\text{od}}}{N_{\text{d}}} \cdot \sqrt{\frac{\Delta H_{\text{s,d}}}{\Delta H_{\text{s,od}}}} - 1 \right)^2$$
(26)

$$P_{\text{in,od}} = \sqrt{q_{\text{m,in,od}}^2 T_{\text{in,od}} Y_{\text{d}} + P_{\text{out,od}}^2}$$
 (27)

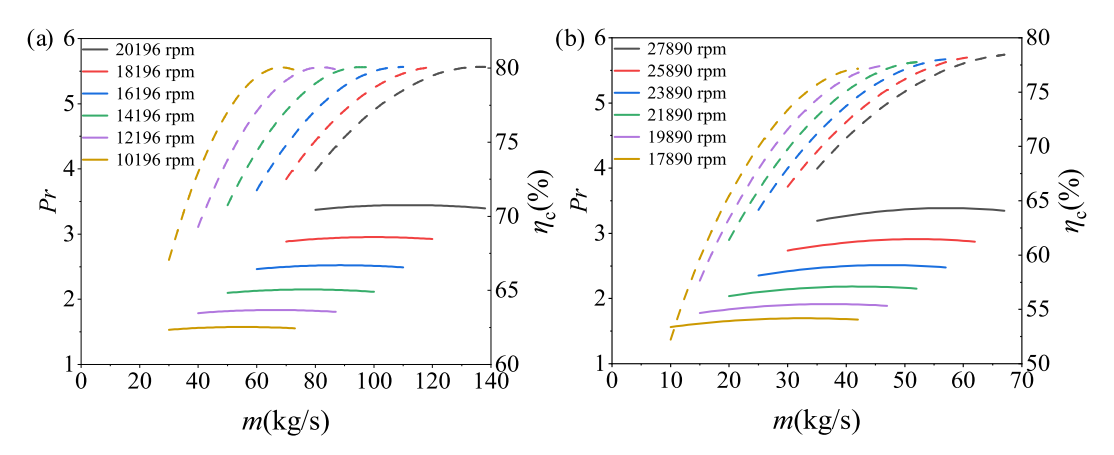


Fig. 3. Main compressor performance curve (a), recompressor performance curve (b), the solid line represents the pressure ratio and the dotted line represents the efficiency.

where η_T is the isentropic efficiency of turbine; ΔH is the enthalpy drop; and N is the turbine speed.

3.4. Cycle part-load calculation model

The models for the heat exchanger, compressor, and turbine are coded using MATLAB software, with the components interconnected to simulate the sCO₂ cycle. The flowchart for the part-load model of IC is depicted in Fig. 4(a). The process begins with inputting the load demand, structural parameters of each major component, and known parameters of the cycle. Initially, assumptions are made regarding the total flow rate and pressure drop across the recuperator, which determine the pressure at each point in the cycle. Subsequently, the turbine outlet temperature T_6 is calculated using the turbine off-design model. Assuming outlet temperatures T_7 and T_8 for the HTR and LTR respectively, the compressor outlet temperature and isentropic efficiency are determined using the compressor off-design model. Next, the recuperator outlet temperatures and pressure drops are computed using the heat exchanger off-design model. Finally, the total flow rate is recalculated based on the given load demand. The calculation is considered complete when the heat exchanger temperatures, pressure drops, and total flow rate converge. If convergence is not achieved, the assumptions are readjusted accordingly.

The flowchart for the part-load model of IDC is depicted in Fig. 4(b). The process begins with inputting the load demand, structural parameters of each major component, and known parameters of the cycle. Initially, the flow rate of the SC1 cycle is assumed, and the part-load model of IC is used to calculate the net work of the SC1 cycle $W_{\rm net,SC1}$ and the high-pressure side outlet temperature T_{3a} of the LTR(a). Following this, assuming the flow rate of the SC2 cycle, the part-load model of IC is utilized again to compute the net work of the SC2 cycle $W_{\rm net,SC2}$ and the high-pressure side outlet temperature T_{3a} of the LTR (b). The calculation is considered complete when T_{3a} and T_{3a} are equal, and the sum of net work converges. If convergence is not achieved, adjustments are made to the flow rates of SC1 and SC2 accordingly.

3.5. Model validation

The accuracy of the cycle calculation model was verified by comparing the simulation results with reference values reported in the reference (HaoNan et al., 2024) The comparison results are presented in Table 3. Specifically, we selected the parameters provided in reference (HaoNan et al., 2024) to calculate the cycle efficiency and compared our results with the reported values. The results show that the deviation in

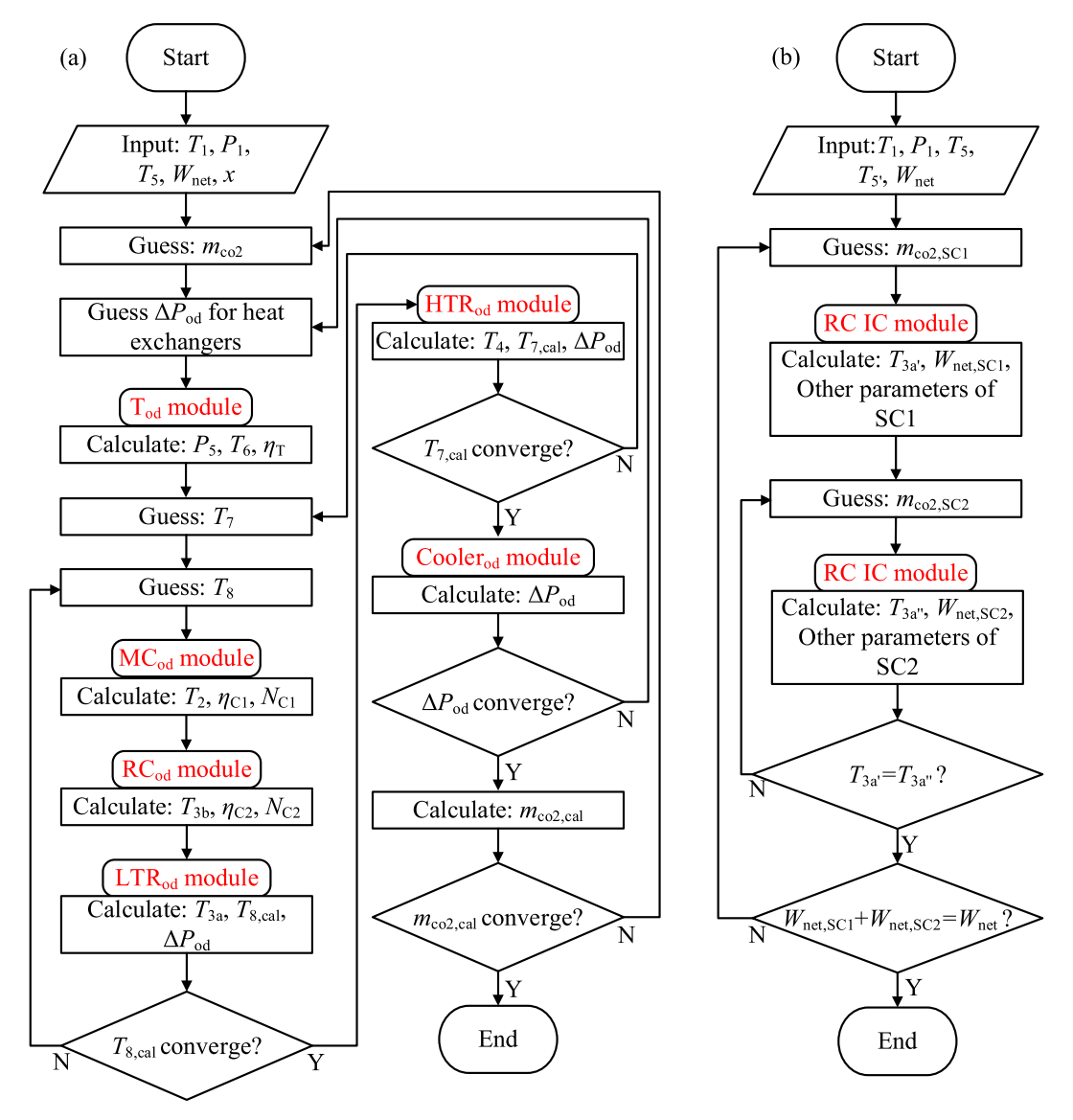


Fig. 4. Flowchart for the part-load model of IC (a) and IDC (b).

Table 3
Accuracy of the model.

Load	Reference (%) (HaoNan et al., 2024)	Calculation (%)	Difference (%)
100 %	49.54	49.59	0.06
90 %	49.78	49.80	0.02
80 %	49.69	49.73	0.04
70 %	49.39	49.36	0.03
60 %	48.69	48.66	0.02
50 %	47.46	47.40	0.06
40 %	45.43	45.44	0.02
30 %	42.24	42.29	0.05

cycle efficiency is within 0.06 %, indicating that the computational model used in this study is reliable and the simulation results are credible.

4. Results and discussion

In order to further analyze the efficiency advantages of IDC control strategy at part-load, this paper takes the $20~\mathrm{MW}~\mathrm{sCO_2}$ recompression cycle and the decoupling cycle as a reference to conduct a comparative analysis of the cycle thermal efficiency and the performance of each equipment. Fig. 1 illustrates the schematic diagrams of both types of cycles. The cycle employs $\mathrm{CO_2}$ storage tanks to adjust the mass flow rate for load regulation. A printed circuit heat exchanger (PCHE) is utilized in the recuperator and cooler, with water serving as the cooling fluid in the cooler. Parameters for the design of the $\mathrm{sCO_2}$ cycle are detailed in Table 4 (Jinliang et al., 2023).

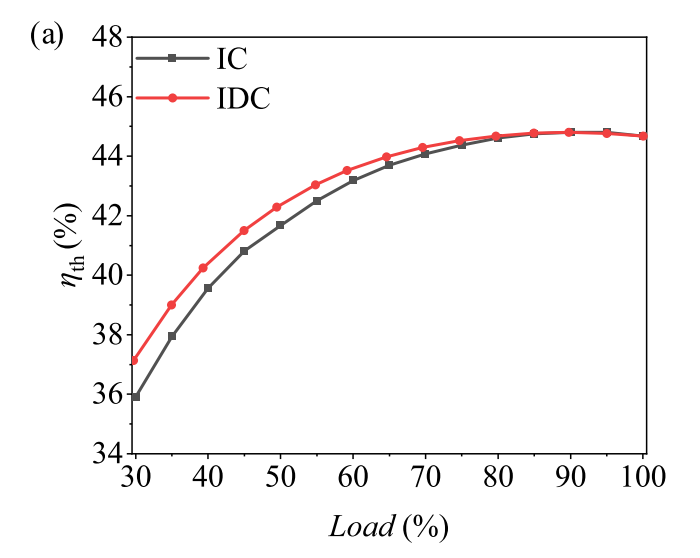
The assumptions for the calculations are outlined as follows: 1. The part-load performance is computed under steady-state conditions (Yang et al., 2020). 2. Both the turbine and the generator maintain a constant speed, while the main compressor and the recompressor can operate at variable speeds (Dostal, 2004). 3. The split ratio remains constant at part-load. 4. The study focuses on a generalized sCO₂ cycle with a generalized heat source capable of providing sufficient heat at part-load. 5. The cooler can supply sufficient cooling fluid to maintain a consistent state at the inlet of the main compressor (Fan and Dai, 2021). 6. Heat transfer between the cycle and the surroundings is neglected.

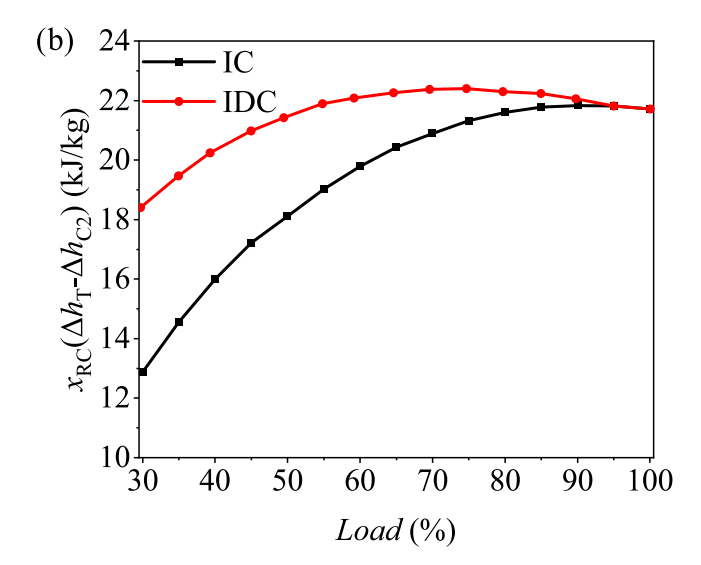
4.1. Analysis of cycle thermal efficiency

The cycle thermal efficiencies of IC and IDC at part-load are depicted in Fig. 5(a). As the load decreases, the efficiency advantage of adopting IDC becomes more pronounced. The maximum difference between the two strategies occurs at 30 % load, with the thermal efficiency of IDC being 1.21 % higher than that of IC. Fig. 5(b) illustrates the variation curve of the net work superimposed term in Eq. (9) at part-load. Compared to IC, the net work superimposed term of IDC is higher, and as the load decreases, the difference between the two strategies gradually increases, reaching its peak difference at 30 % load, which amounts to $5.52~{\rm kJ/kg}$. This variation pattern aligns with the difference in cycle

Table 4 Parameters for sCO₂ cycle design.

Parameters	Value	Parameters	Value
Net power W_{net}	20 MW	Cooler pressure drop ΔP_{Cooler}	150 kPa
Turbine inlet temperature T_5 , T_5 '	605 °C	Isentropic efficiency of turbine η_{T1}	87.00 %
Turbine inlet pressure P_5 , $P_{5'}$	27 MPa	Isentropic efficiencies of main compressor η_{C1}	80.00 %
Main compressor inlet temperature T_1	32 °C	Isentropic efficiencies of recompressor η_{C2}	78.40 %
Main compressor inlet pressure P_1	8.1 MPa	Max pressure drop of recuperator $\Delta P_{\rm R}$	150 kPa
Heater pressure drop $\Delta P_{\mathrm{Heater}}$	500 kPa	Pinch temperature of recuperator $\Delta T_{\rm R}$	10 °C





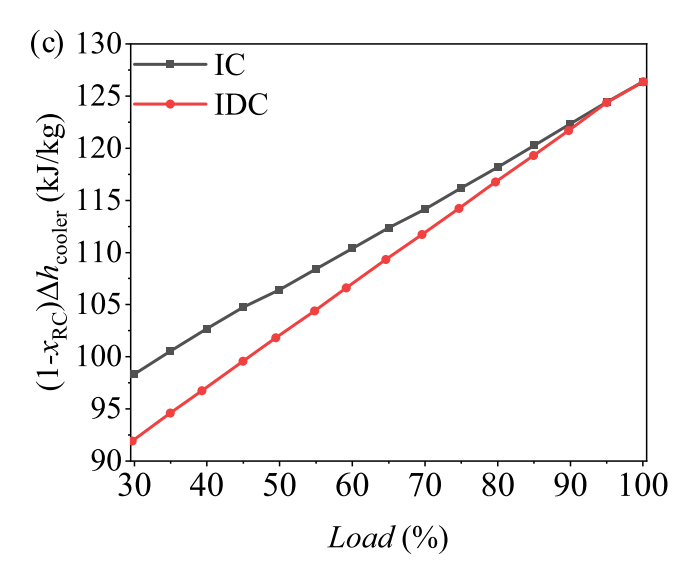


Fig. 5. Variation curve of cycle thermal efficiency (a), network superimposed term (b) and enthalpy drop in the cooler (c) with load adopting IC and IDC.

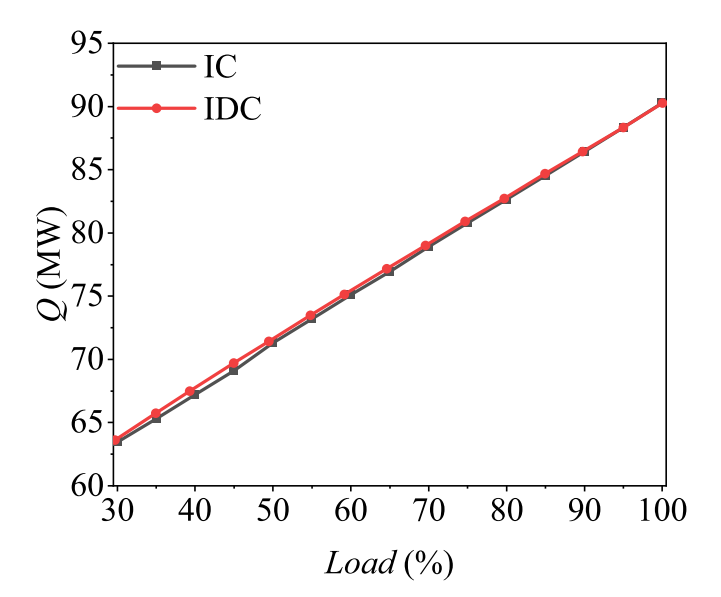
thermal efficiency between the two strategies. Fig. 5(c) shows the variation curve of enthalpy drop in the cooler at part-load. In comparison with IC, the enthalpy drop in the cooler of IDC is reduced. This reduction indicates an increase in the value of the base cycle term in Eq. (9) with the new control strategy. The variation patterns observed in the net work superposition term and the enthalpy drop in the cooler align with the net power superposition principle and the analysis of cycle thermal efficiency mentioned in Part 2. This supports the conclusion that cycle thermal efficiency is enhanced with the adoption of IDC.

To further demonstrate the reasons for the increased efficiency of adopting IDC strategy, the performance of the three main components of the cycle, the recuperator, the compressor, and the turbine, will be illustrated.

4.2. Part-load operation characteristics of the recuperator system

The amount of heat dissipated in the cooler is closely linked to the regenerative system. Fig. 6 illustrates the variation of total regenerative heat with load adopting the two strategies. While the total regenerative heat remains nearly equal between the two strategies, the distribution of regenerative heat among each recuperator is altered by the different control strategies. The proportion of regenerative heat from each recuperator to the total regenerative heat at 30 % load is depicted in Fig. 7. Since the RC cycle has only two recuperators, it is considered as having four recuperators according to the corresponding splitting ratios (Sun et al., 2020). It's evident that after adopting IDC, the regenerative heat of HTR(b) remains almost constant. However, the regenerative heat of LTR(a) and LTR(b) increases by 4.2 % and 2.2 %, respectively, while the regenerative heat of HTR(a) decreases by 6.7 %.

The increasing regenerative heat of LTR(b) indicates that SC1 receives more regenerative heat from SC2. This is due to the adoption of IDC, which results in a higher inlet temperature of the LTR(b) low-pressure side. Fig. 8(a) depicts the variation curves of LTR and LTR(b) low-pressure side inlet temperature with load adopting IC and IDC. It's evident that $T_{7'}$ with IDC is greater than T_{7} with IC. Higher inlet temperatures of the low-pressure side result in more regenerative heat in LTR(b). Additionally, the temperature difference for heat transfer inside LTR(b) is improved. Fig. 9 illustrates the T-Q distributions of LTR and LTR(b) at 30 % load. The log mean temperature differences before and after the adoption of IDC are 7.00 °C and 4.79 °C, respectively. The temperature difference between the two sides of LTR(b) is significantly smaller than that between the two sides of LTR, resulting in more



 $\begin{tabular}{ll} Fig. 6. Variation curve of total regenerative heat with load adopting IC and IDC. \end{tabular}$

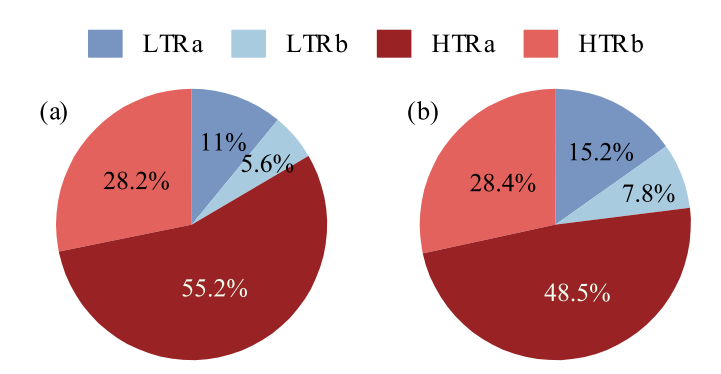


Fig. 7. Proportion of regenerative heat of each recuperator to total regenerative heat adopting IC (a) and IDC (b).

efficient heat transfer. Moreover, the increase in regenerative heat of LTR(b) leads to an increase in its high-pressure side outlet temperature T_{3a} , as depicted in Fig. 8(b). As T_{3a} rises, the regenerative heat of HTR(a) decreases, resulting in an increase in its low-pressure side outlet temperature T_7 . As shown in Fig. 8(a), it can be observed that T_7 which adopts IDC is greater than T_7 which adopts IC The reduced regenerative heat of HTR(a) is recovered in LTR(a), explaining the increased regenerative heat of LTR(a). The redistribution of regenerative heat in the recuperator system, combined with the adoption of IDC to independently control the flow rate of each sub-cycle, significantly contributes to reducing the heat dissipation in the cooler, denoted as $(1-x_{RC})\Delta h_{Cooler}$ in Eq. (9).

4.3. Part-load operation characteristics of compressor systems

The variation curve of compressor efficiency with load using the two strategies is illustrated in Fig. 10(a). During the transition from $100\,\%$ load to $30\,\%$ load, the main compressor efficiency decreased by $1.89\,\%$ and the recompressor efficiency decreased by $4.04\,\%$ with IC. In contrast, with IDC, the main compressor efficiency decreased by $2.07\,\%$ and the recompressor efficiency decreased by $3.03\,\%$. It's observed that by adopting IDC at part-load, the efficiency drop of the main compressor increases slightly, but conversely, the efficiency drop of the recompressor decreases significantly. This allows the compressor to operate closer to the design conditions without excessive deviation, thereby generally improving compressor operating efficiency and safety.

The observed phenomenon results from the fact that adopting IDC changes the flow rates of the compressors. As shown in Fig. 10(b), during the transition from 100 % to 30 % load, when adopting IC, the flow rate ratios of both the main compressor and the recompressor decrease by 44.59 %; when adopting IDC, the main compressor flow rate ratio decreases by 47.25 %, and the recompressor by 37.61 %. According to the compressor performance curves shown in Fig. 3, the greater variation in the main compressor flow rate when adopting IDC leads to a reduction in its efficiency, while the recompressor efficiency improves.

4.4. Part-load operation characteristics of the turbine system

The curves illustrating the variation of turbine outlet temperature and regenerative heat per unit mass flow rate of the low-pressure side fluid with load are depicted in Fig. 11(a and b). As the load decreases, the turbine outlet temperature gradually increases, which is attributed to the decrease in turbine efficiency. Meanwhile, the regenerative heat per unit mass flow rate on the low-pressure side increases continuously, and this trend corresponds to the increase in turbine outlet temperature. This is because a higher outlet temperature allows the fluid entering the recuperator to release more thermal energy. This indicates that as the turbine deviates from its design conditions, its isentropic efficiency decreases on the one hand, while on the other hand, it positively impacts the regenerative heat of the cycle.

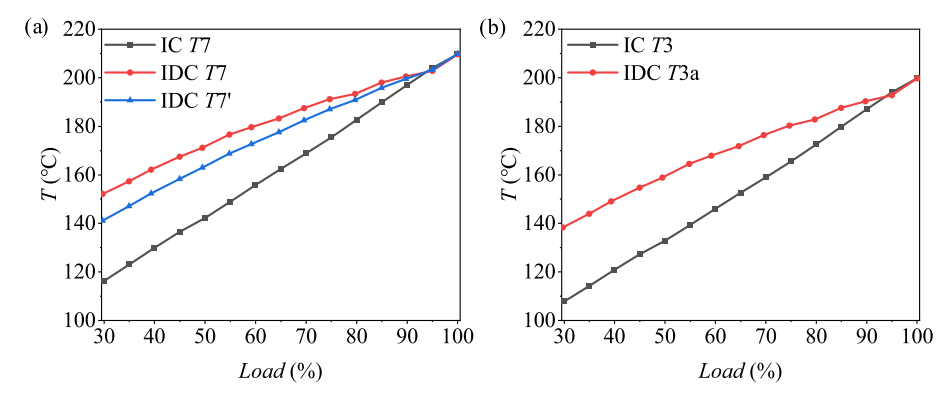


Fig. 8. Variation curve of T_7 , $T_{7'}$ (a) and T_3 , T_{3a} (b) with load adopting IC and IDC.

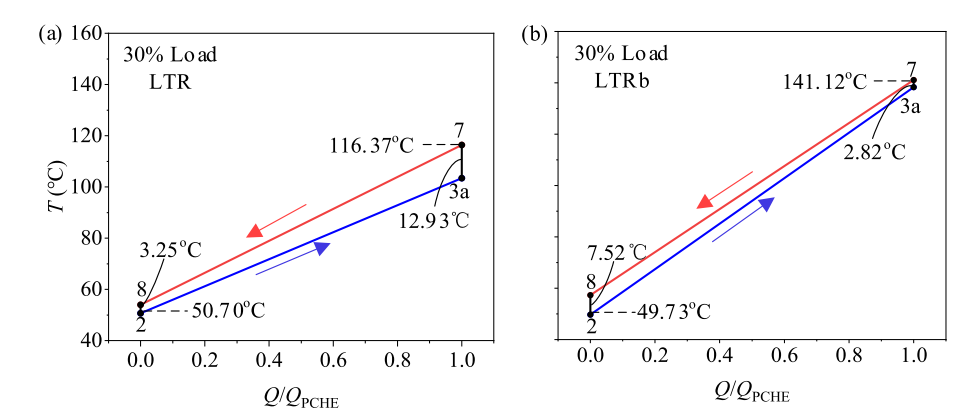


Fig. 9. T-Q distribution of LTR (left) and LTR (b) (right) at 30% loading.

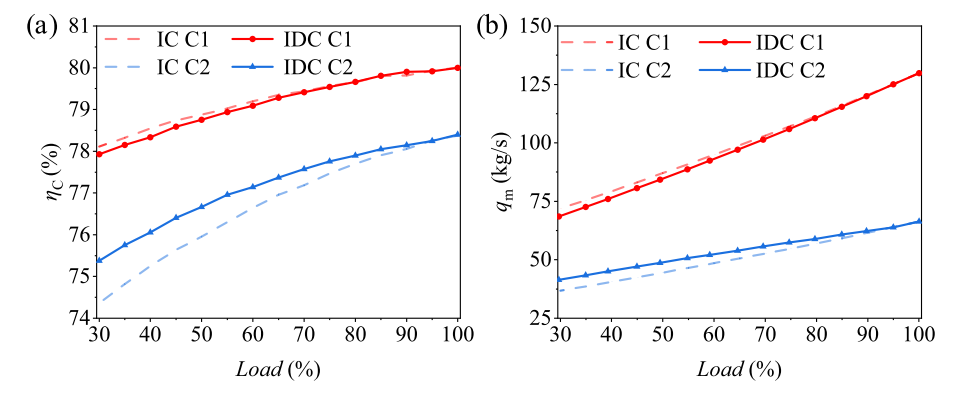


Fig. 10. Variation of compressor efficiency (a) and mass flow rate (b) with load adopting IC and IDC.

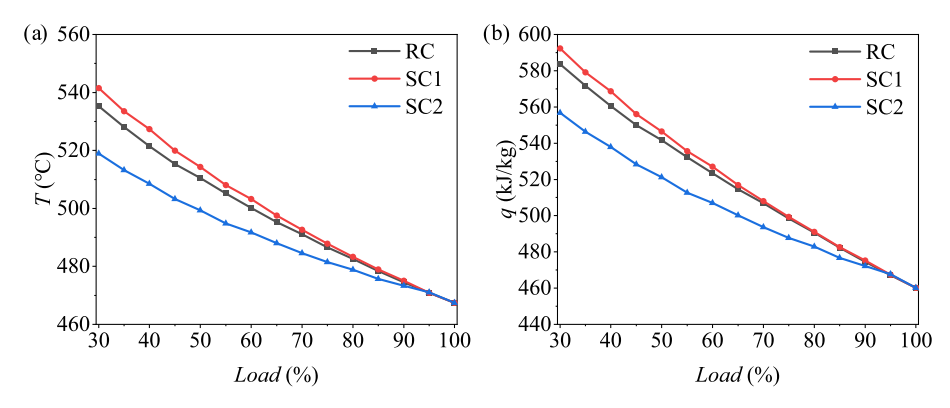


Fig. 11. Variation curves of turbine outlet temperature (a) and regenerative heat of low-pressure side fluid (b) with load adopting IC and IDC.

It's worth noting that after decoupling the RC cycle, the cycle transitions from a single turbine T1 within RC to two smaller-capacity turbines T1(a) and T1(b) within SC1 and SC2. The reduction in turbine capacity inevitably leads to a decrease in turbine efficiency, negatively impacting cycle thermal efficiency. However, this decrease in turbine efficiency causes the turbine outlet temperature to rise, positively impacting the regenerative heat of the cycle. Therefore, it's necessary to analyze the specific trend of cycle thermal efficiency considering the combined effect of these factors. Fig. 12 compares the cycle thermal efficiency with two strategies at different turbine rated efficiencies. The reduction in turbine rated efficiency results in the thermal efficiency of the decoupled cycle being lower than that of the RC cycle at 100 % load. However, as the load decreases, the thermal efficiency decreases more slowly when adopting IDC, leading to a reversal in the comparison of thermal efficiencies at part-load. It can be observed that when the rated efficiency of T1(a) is 85 % and that of T1(b) is 83 %, the thermal efficiencies at 30 % load are nearly equal for both control strategies. If the rated efficiencies are further reduced, the thermal efficiency of the IDC will become lower than that of the IC at part-load. Therefore, the efficiency advantage of IDC at part-load depends on the turbine capacity. If the turbine capacity is larger both before and after decoupling, and its rated efficiency decreases less or remains constant, then there is an efficiency advantage of IDC. Otherwise, there is no efficiency advantage of IDC.

4.5. Influence of minimum cycle temperature

The minimum temperature of the cycle has a critical impact on overall performance. As demonstrated in previous studies, an increase in the minimum cycle temperature results in a decrease in cycle efficiency (Ehsan et al., 2018). This effect also applies to the IDC. As shown in Fig. 13, at 60 % load, the cycle efficiency under two different control strategies is compared across a range of minimum cycle temperatures. It can be observed that as the minimum temperature increases, the efficiency decreases for both strategies. However, the IDC consistently achieves higher efficiency, with the efficiency difference remaining above 0.3 % across all conditions. This further confirms the superiority of the IDC in part-load operation.

4.6. Future scope and recommendations

The inventory decoupling control strategy combines inventory

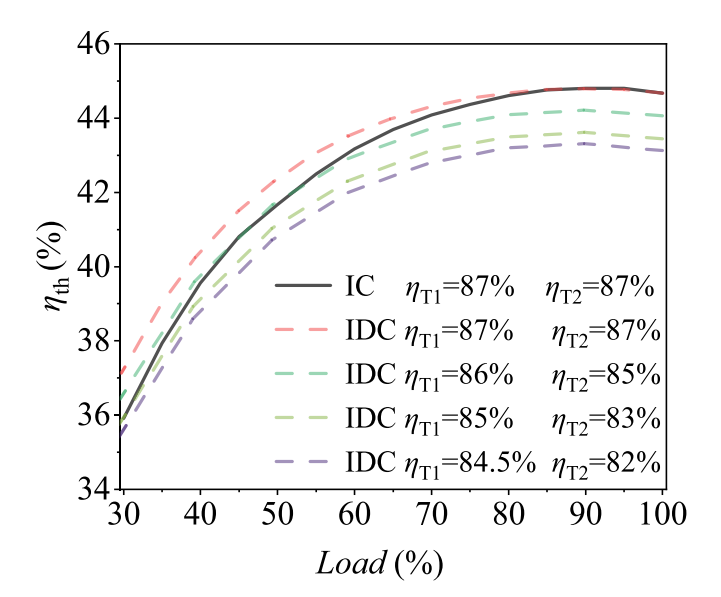


Fig. 12. Comparison of cycle thermal efficiency with two strategies at different turbine rated efficiencies.

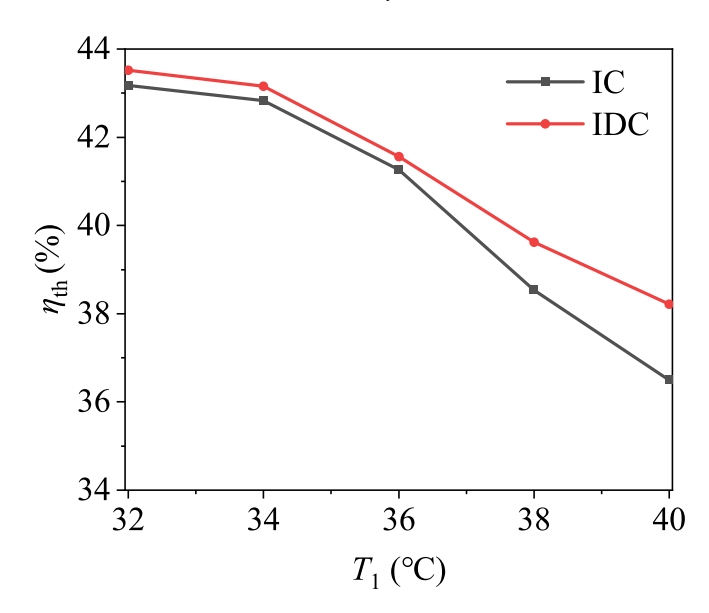


Fig. 13. Cycle thermal efficiency corresponding to different minimum cycle temperatures at 60% load.

control with cycle configuration, resulting in a novel decoupled cycle and a more efficient part-load control strategy. Similar to inventory control under varying loads, it requires managing the $\rm CO_2$ storage tank to adjust the working fluid flow, and it is relatively simple to implement for variable load control. Moreover, compared to inventory control, the cycle load control in this strategy is more flexible and efficient, offering a higher degree of feasibility.

The potential challenges and limitations of the IDC are primarily as follows: 1. Whether the thermal load provided by the heat source is sufficient to meet the requirements of both sub-cycles. Additionally, there is a temperature discrepancy between the heat absorption zones of the two sub-cycles, which necessitates optimizing the heat source structure. 2. After decoupling the recompression cycle, the turbine capacity decreases, resulting in lower turbine efficiency. If the turbine's rated efficiency decreases significantly, the IDC may lose its advantages.

To address these issues, future research will focus on optimizing the heat source structure. Furthermore, efforts will be made to refine the IDC to mitigate the impact of turbine efficiency losses.

5. Conclusions

In this study, the partial-load characteristics of the cycle are analyzed in conjunction with the cycle construction process, and the potential of inventory control is further explored. Based on the net power superposition principle, we proposed a new strategy from the perspective of cycle configuration optimization: by decoupling the cycle and applying independent inventory control to each sub-cycle, a more efficient partial-load control strategy is obtained. The main conclusions are as follows:

- In this study, the thermal efficiency of the recompression cycle is mathematically derived based on the net power superposition principle, thereby extending the application of this principle to the field of part-load analysis. Accordingly, an efficiency enhancement approach for sCO₂ cycles under partial-load operation is proposed:

 When the base cycle term remains constant, a large net power superposition term results in higher thermal efficiency.
 When the power superposition term remains constant, a larger base cycle term results in higher thermal efficiency.
- A new part-load control strategy is proposed based on a new idea: the inventory decoupling control strategy. This strategy can simultaneously improve the base cycle efficiency and the net power

- superposition at part-load. Further, by constructing a part-load model of a 20 MW sCO $_2$ cycle, it is demonstrated that the new strategy can enhance the cycle thermal efficiency by 1.21 % at 30 % load.
- 3. The IDC strategy alters the distribution of the regenerative heat inside each recuperator. The SC2 cycle supplies more regenerative heat to the SC1 cycle, with an increase of 2.2 %. The internal heat transfer inside the LTR(b) is more efficient, with a log mean temperature difference of 4.79 °C. Additionally, due to the change of the LTR(a) low-pressure side inlet temperature T_7 , the amount of regenerative heat in the LTR(a) increases, while the amount of regenerative heat in the HTR(b) decreases accordingly.
- 4. The adoption of IDC strategy results in a much smaller change in the overall compressor efficiency and an overall improvement in compressor operating efficiency and safety. The decrease in turbine efficiency at part-load has a positive impact on the regenerative heat of the cycle. In addition, to assess the impact of reduced turbine capacity on the decoupling cycle, the changes in thermal efficiency of the decoupling cycle at different turbine rated efficiencies are calculated. In cases where the difference in turbine efficiency before and after decoupling falls within the range of 2–4 %, the IDC strategy shows an efficiency advantage.

CRediT authorship contribution statement

Cheng Chang: Writing – original draft, Software, Data curation. Enhui Sun: Supervision, Methodology. Jinliang Xu: Writing – review & editing, Conceptualization. Xiaoming Zhang: Methodology, Conceptualization. Huan Ye: Supervision, Methodology. Qichen Qian: Visualization, Investigation.

Declaration of competing interest

The authors declare that they have no known competing financial interests or personal relationships that could have appeared to influence the work reported in this paper.

Acknowledgements

The research was supported by the Natural Science Foundation of China (52130608, 52206010).

Data availability

Data will be made available on request.

References

- Ehsan, M.M., Guan, Z., Klimenko, A.Y., 2018. A comprehensive review on heat transfer and pressure drop characteristics and correlations with supercritical CO2 under heating and cooling applications[J]. Renew. Sustain. Energy Rev. 92, 658–675.
- Ehsan, M.M., Awais, M., Lee, S., et al., 2023. Potential prospects of supercritical CO2 power cycles for commercialisation: applicability, research status, and advancement [J]. Renew. Sustain. Energy Rev. 172, 113044.
- Açıkkalp, E., 2017. Ecologic and sustainable objective thermodynamic evaluation of molten carbonate fuel cell-supercritical CO2 Brayton cycle hybrid system[J]. Int. J. Hydrogen Energy 42 (9), 6272–6280.
- Mecheri, M., Le Moullec, Y., 2016. Supercritical CO2 Brayton cycles for coal-fired power plants[J]. Energy 103, 758–771.
- Zhang, F., Liao, G., E j., et al., 2021. Comparative study on the thermodynamic and economic performance of novel absorption power cycles driven by the waste heat from a supercritical CO2 cycle[J]. Energ. Conver. Manage. 228, 113671.
- Linares, J.I., Montes, M.J., Cantizano, A., et al., 2020. A novel supercritical CO2 recompression Brayton power cycle for power tower concentrating solar plants[J]. Appl. Energy 263, 114644.
- Dal Cin, E., Lazzaretto, A., Toffolo, A., 2023. A novel extension of the SYNTHSEP methodology for the optimal synthesis and design of supercritical CO2 cycles in waste heat recovery applications[J]. Energ. Conver. Manage. 276, 116535.
- Ryu, J.Y., Ar, K.o., Park, S.H., et al., 2020. Thermo-economic assessment of molten carbonate fuel cell hybrid system combined between individual sCO2 power cycle and district heating[J]. Appl. Therm. Eng. 169, 114911.

- Ehsan, M.M., Guan, Z., Gurgenci, H., et al., 2020. Feasibility of dry cooling in supercritical CO2 power cycle in concentrated solar power application: review and a case study[J]. Renew. Sustain. Energy Rev. 132, 110055.
- Monjurul Ehsan, M., Duniam, S., Li, J., et al., 2020. A comprehensive thermal assessment of dry cooled supercritical CO2 power cycles[J]. Appl. Therm. Eng. 166, 114645.
- Ehsan, M.M., Wang, X., Guan, Z., et al., 2018. Design and performance study of dry cooling system for 25 MW solar power plant operated with supercritical CO2 cycle [J]. Int. J. Therm. Sci. 132, 398–410.
- Ehsan, M.M., Duniam, S., Guan, Z., et al., 2019. Seasonal variation on the performance of the dry cooled supercritical CO2 recompression cycle[J]. Energ. Conver. Manage. 197, 111865.
- Monjurul Ehsan, M., Guan, Z., Gurgenci, H., et al., 2020. Novel design measures for optimizing the yearlong performance of a concentrating solar thermal power plant using thermal storage and a dry-cooled supercritical CO2 power block[J]. Energ. Conver. Manage. 216, 112980.
- Floyd, J., Alpy, N., Moisseytsev, A., et al., 2013. A numerical investigation of the sCO2 recompression cycle off-design behaviour, coupled to a sodium cooled fast reactor, for seasonal variation in the heat sink temperature[J]. Nucl. Eng. Des. 260, 78–92.
- Duniam, S., Veeraragavan, A., 2019. Off-design performance of the supercritical carbon dioxide recompression Brayton cycle with NDDCT cooling for concentrating solar power[J]. Energy 187, 115992.
- Correa, F., Barraza, R., Soo Too, Y.C., et al., 2021. Optimized operation of recompression sCO2 Brayton cycle based on adjustable recompression fraction under variable conditions[J]. Energy 227, 120334.
- Gini, L., Maccarini, S., Traverso, A., et al., 2023. A prototype recuperated supercritical co2 cycle: part-load and dynamic assessment[J]. Appl. Therm. Eng. 225, 120152.
- HaoNan, Z.H.E.N.G., JinLiang, X.U., ZhaoFu, W.A.N.G., et al., 2024. Partial loadoperation characteristics of the sCO2 cycle (in Chinese)[J]. Sci. Sin. Technol. 54 (1), 78–90.
- Yang, J., Yang, Z., Duan, Y., 2020. Part-load performance analysis and comparison of supercritical CO2 Brayton cycles[J]. Energ. Conver. Manage. 214, 112832.
- Ma, T., Li, M.J., Xu, J.L., et al., 2022. Study of dynamic response characteristics of S-CO2 cycle in coal-fired power plants based on real-time micro-grid load and a novel synergistic control method with variable working conditions[J]. Energ. Conver. Manage, 254, 115264.
- Wang, R., Wang, X., Shu, G., et al., 2022. Comparison of different load-following control strategies of a sCO2 Brayton cycle under full load range UI. Energy 246, 123378.
- strategies of a sCO2 Brayton cycle under full load range[J]. Energy 246, 123378. Li, H., Fan, G., Cao, L., et al., 2020. A comprehensive investigation on the design and off-design performance of supercritical carbon dioxide power system based on the small-scale lead-cooled fast reactor[J]. J. Clean. Prod. 256, 120720.
- Ming, Y., Tian, R., Zhao, F., et al., 2023. Control strategies and transient characteristics of a 5MWth small modular supercritical CO2 Brayton-cycle reactor system[J]. Appl. Therm. Eng. 235, 121302.
- Luu, M.T., Milani, D., McNaughton, R., et al., 2018. Advanced control strategies for dynamic operation of a solar-assisted recompression supercritical CO2 Brayton power cycle[J]. Appl. Therm. Eng. 136, 682–700.
- Singh, R., Kearney, M.P., Manzie, C., 2013. Extremum-seeking control of a supercritical carbon-dioxide closed Brayton cycle in a direct-heated solar thermal power plant[J]. Energy 60, 380–387.
- Heifetz, A., Vilim, R., 2015. Turbine Bypass, Mass Inventory, and Mixed-Mode Generator Power Control of S-CO2 Recompression Cycle[J]. Nucl. Technol. 189 (3), 268–277.
- Fan, G., Li, H., Du, Y., et al., 2020. Preliminary design and part-load performance analysis of a recompression supercritical carbon dioxide cycle combined with a transcritical carbon dioxide cycle[J]. Energ. Conver. Manage. 212, 112758.
- Oh, B.S., Ahn, Y.H., Yu, H., et al., 2017. Safety evaluation of supercritical CO2 cooled micro modular reactor[J]. Ann. Nucl. Energy 110, 1202–1216.
- Du, Y., Yu, Z., Yang, C., et al., 2024. Comprehensive evaluation of part-load exergy performance of a supercritical carbon dioxide recompression cycle controlled by various strategies[J]. Energ. Conver. Manage. 301, 118013.
- Sun, E., Xu, J., Li, M., et al., 2020. Synergetics: the cooperative phenomenon in multi-compressions S-CO2 power cycles[J]. Energy Convers. Manage.: X 7, 100042.
- Hangning, L.I., Enhui, S.U.N., Jinliang, X.U., 2020. Construction and analysis of supercritical carbon dioxide cycle with multi-stage regenerative-compression (in Chinese)[J]. Proc. CSEE 40 (S1), 211–221.
- Jiang, Y., Liese, E., Zitney, S.E., et al., 2018. Design and dynamic modeling of printed circuit heat exchangers for supercritical carbon dioxide Brayton power cycles[J]. Appl. Energy 231, 1019–1032.
- Chu, W.x., Li, W.x., Ma, T., et al., 2017. Experimental investigation on SCO2-water heat transfer characteristics in a printed circuit heat exchanger with straight channels[J]. Int. J. Heat Mass Transf. 113, 184–194.
- Pierres, R.L, Southall, D., Osborne, S., 2011. Impact of mechanical design issues on printed circuit heat exchangers[C]. In: Proceedings of SCO2 Power Cycle Symposium. Bolder, pp. 24–25.
- Dyreby, J.J. Modeling the supercritical carbon dioxide brayton cycle with recompression [D]. In: ProQuest Dissertations and Theses. United States Wisconsin: The University of Wisconsin Madison.
- Enhui, S.U.N., Zhenyu, Y.A.N.G., Kailong, L.I.A.O., et al., 2023. Design and performance prediction of supercritical carbon dioxide centrifugal compressor (in Chinese)[J]. Therm. Power Gener. 52 (6), 127–134, 156.
- Gabbrielli, R., 2012. A novel design approach for small scale low enthalpy binary geothermal power plants[J]. Energ. Conver. Manage. 64, 263–272.

Fan, G., Dai, Y., 2021. Thermo-economic optimization and part-load analysis of the combined supercritical CO2 and Kalina cycle[J]. Energ. Conver. Manage. 245, 114572 Jinliang, X.U., He, T.I.A.N., Enhui, S.U.N., et al., 2023. One dimensional design of small capacity supercritical CO2 coal fired power generation system and analysis of regenerator compactness (in Chinese)[J]. J. China Coal Soc. 48 (1), 438–451.

Dostal, V., 2004. A supercritical carbon dioxide cycle for next generation nuclear reactors [D]. Massachusetts Institute of Technology.